PCCP

Polyradical Character Assessment using Multireference Calculations and Comparison with Density-Functional Derived Fractional Occupation Number Weighted Density Analysis

Journal:	*Physical Chemistry Chemical Physics*
Manuscript ID	CP-ART-08-2023-003734.R1
Article Type:	Paper
Date Submitted by the Author:	25-Sep-2023
Complete List of Authors:	Nieman, Reed; Texas Tech University, Dep. Chemistry and Biochemistry Carvalho, Jhonatas; Texas Tech University, Department of Chemistry and Biochemistry Jayee, Bhumika; Texas Tech University, Department of Chemistry and Biochemistry Hansen, Andreas; University of Bonn, Mulliken Center for Theoretical Chemistry Aquino, Adelia; University of Vienna, Kertesz, Miklos; Georgetown University, Department of Chemistry Lischka, Hans; University of Vienna, Institute for Theoretical Chemistry and Structural Biology

Polyradical Character Assessment using Multireference Calculations and Comparison with Density-Functional Derived Fractional Occupation Number Weighted Density Analysis

Reed Nieman,[1,a] Jhonatas R. Carvalho,[1,a] Bhumika Jayee,[1,a,b] Andreas Hansen,[2] Adelia J. A. Aquino,[3] Miklos Kertesz,[4] Hans Lischka[1]*

[1]Department of Chemistry and Biochemistry, Texas Tech University, Lubbock, TX 79409-1061, USA

[2] Mulliken Center for Theoretical Chemistry, Universität Bonn, D- 53115 (Germany)

[3]Department of Mechanical Engineering, Texas Tech University, Lubbock, TX 79409-1061, USA

[4]Chemistry Department and Institute of Soft Matter, Georgetown University, Washington, District of Columbia 20057-1227, USA

[a] These authors contributed equally to this publication.

[b] Current address: Department of Chemistry and Chemical Biology, Northeastern University, Boston MA, 02115, USA

* email: Hans.Lischka@ttu.edu

Abstract

The biradicaloid character of different types of polycyclic aromatic hydrocarbons (PAHs) based on small band gaps is an important descriptor to assess their opto-electronic properties. In this work, the unpaired electron densities and numbers of unpaired electrons (N_U values) calculated at the high-level multireference averaged quadratic coupled-cluster (MR-AQCC) method are used to develop a test set to assess the capabilities of different biradical descriptors based on density functional theory. A benchmark collection of 29 different compounds has been selected. The DFT descriptors contain primarily the fractional occupation number weighted electron density (FOD) based on simplified thermally-assisted-occupation density functional theory (TAO-DFT) calculations, but the singlet-triplet energy difference and other descriptors denoted as y_0 and n_{LUNO} have been considered as well. After adjustment of the literature-recommended finite temperatures, a very good, detailed agreement between unpaired density and FOD analysis is observed which is also manifested in excellent statistical correlations. The other two descriptors also show good correlations even though the absolute scaling is not satisfactory. A new linear fit of FOD data to the MR-AQCC reference values leads to an improved regression relation for determining the recommended finite temperature value in dependence of the Hartree-Fock exchange. This provides the basis for fast and reliable assessment of the biradical character of many classes of PAHs without the need for performing computationally extended MR calculations.

1. INTRODUCTION

Graphene is a zero-bandgap material with a wide range of applications.[1, 2] Cutting a graphene sheet into nanosized fragments produces nanographenes which contain units of polycyclic aromatic hydrocarbons (PAHs).[3] In many cases PAHs possess significant open-shell character in the singlet ground state[4-10] which leads to remarkable opto-electronic properties due to small band gaps of these PAHs. These systems have not played significant roles in the future of photovoltaic devices in terms of singlet-fission,[11, 12] but have also reported promising results for organic light emitting device (OLED) materials.[13-15] Advancements in the field of molecule-based batteries[13, 16] and field-effect transistors[17, 18] have been investigated owing to the molecular-sized open-shell graphene fragments.

Quantum chemical calculations have been found useful to provide the required quantitative characterization of the biradicaloid PAHs. While the computationally efficient density functional theory (DFT) performs quite reliably for closed shell cases, the choice of the density functional still remains a nontrivial step and the method may suffer from spin-contamination effects especially in the important case of broken-symmetry singlet states of biradical molecules.[19, 20] To judge the applicability of DFT methods in such cases, it is necessary to have reliable reference data from accurate methods capable of accounting for the multireference (MR) character of the electronic wave function which is often associated with radical and open shell systems. It has been shown that many of such compounds have two or more dominant contributing electronic configurations with similar weights, as shown by the work of Salem and Roland,[21] and Bonacic-Koutecky, Koutecky, and Michl.[22] MR methods have proven to be flexible and practical in describing such complex systems in a balanced way.[23] They are free of the previously mentioned spin contamination effects and include quasi-degenerate configurations as a basis of characterizing radical and biradicaloid molecules forming the choice of an appropriate reference space. The MR-averaged quadratic coupled-cluster (MR-AQCC) method[24] has been especially reliable as it includes size-consistency contributions.[23] It has been used extensively in calculations of biradicaloid cases such as acenes,[7] zethrenes,[25, 26] and diindenoacenes.[4]

To date, a popular strategy used to identify biradicaloid PAHs consists in the calculation of the diradical character index (y_0) and its closely related observable property, the singlet/triplet splitting energy gap. For the y index value, two forms exist. Yamaguchi proposed the calculation

from the occupations of the highest occupied natural orbital (NO) and lowest unoccupied NO (HONO and LUNO, respectively),[20, 27] while the LUNO occupation[28] alone can also be a useful biradical descriptor with pros and cons in their applications.[29, 30] These calculations are predominantly performed at DFT level. As an alternative, the number of effectively unpaired electrons (N_U) and the corresponding density[20, 31, 32] has been used to identify significant contributions to the biradicaloid character in a series of PAH systems and has shown to correlate closely with the singlet/triplet energy splitting.[4, 25] A more recent descriptor of radical character is the fractional occupation number weighted electron density (FOD)[33] and the corresponding number of "hot" electrons N_{FOD} suggested by Grimme and Hansen. This method can be considered as simplified adoption of Chai's thermally-assisted-occupation density functional theory (TAO-DFT).[34-36] The latter introduces a fictitious temperature of the reference system to generate fractional orbital occupations via the Fermi-Dirac distribution and it was shown the static correlation is closely related to the entropy contribution. Neglecting the fictitious-temperature-dependent energy functionals leads to the "finite-temperature DFT" method (FT-DFT in the following) adopted in Ref. 33 in the context of the FOD. Note that this is clearly different from Mermin-Kohn-Sham method,[37, 38] which is often also referred to as FT-DFT. FT-DFT in combination with FOD has been used to assess the open-shell biradical character of organic molecules with emphasis on PAHs.[39] In a related spirit, FT-DFT calculations have been used by Liu et al.[40] for evaluating strong correlation for transition-metal complexes.

This work will present benchmark *ab initio* multireference calculations characterizing the radical and biradicaloid character of twenty-nine selected PAH structures representing diverse classes of molecules. The N_U values calculated using the high-accuracy MR-AQCC method are compared to the N_{FOD} values and the descriptors y_0 and n_{LUNO} utilizing a range of density functionals characterized by different contributions of exact Hartree-Fock exchange. The objective of this work is to evaluate the performance of the just-listed open-shell descriptors obtained at DFT level and to provide information about the accuracy of their predictions in comparison to MR-AQCC. Thereby, ways should be shown for dealing with the difficult question, especially of the singlet open-shell character of molecules in a computationally efficient but still reliable way as provided by DFT in comparison to MR-AQCC.

2. BENCHMARK COMPOUNDS

The properties of PAHs have been studied intensively in previous investigations. Pioneering DFT and complete active space self-consistent field (CASSCF) investigations on the biradical structure of acenes have been reported by Bendikov et al.[10] Chai has used the TAO-DFT method[34-36] to systematically study singlet-triplet gaps and other electronic properties in acenes whereas CASSCF calculations have been used to investigate hexacene, zethrene, triangulene and uthrene by Melle-Franco.[41] Phenalenyl and triangulene calculations have been performed by Sandoval-Salinas et al.[42] by means of the restricted active space configuration interaction (RASCI) and spin-flip techniques. The same computational approach has been applied by Pérez-Guardiola et al.[43] to the study of increasingly longer acene chains. As already mentioned above, the open-shell character of *n*-acenes and periacenes has been explored previously[7] with MR-AQCC calculations showing the evolution of strong multiradical character of these *n*-acenes (*n* = 2 to 10). MR-AQCC has been used successfully also for other classes of PAHs such as triangular ones, zethrenes and diindenoacenes.[4, 25]

Based on the experience with these investigations, the following classes of compounds have been selected as benchmark examples. The *n*-acenes with *n* = 4, 6, 8 and 10 (structures **1-4**, Figure 1) were considered in the first place to explore the presence of their multiradical character.

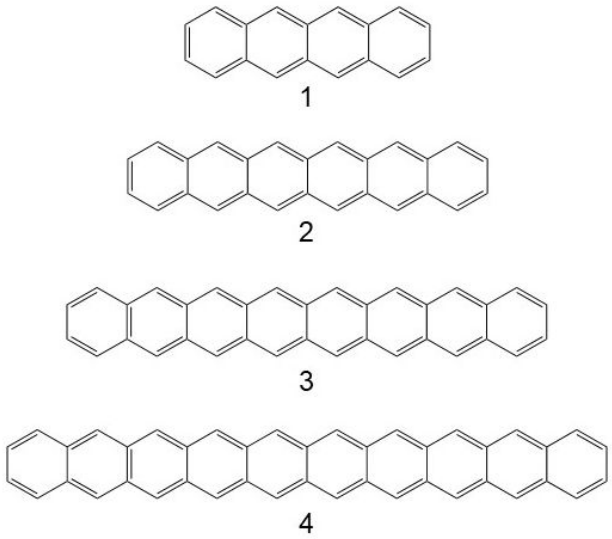

Figure 1. Structures of n-acenes for 4-acene (**1**), 6-acene (**2**), 8-acene (**3**) and 10-acene (**4**).

Cis- and *trans*-diindenoacenes (structures **5-14,** Figure 2) are a class of compounds designed to regulate the biradicaloid character of acenes.[44] They are known for unique chemical properties and high reactivity.[45] These compounds have been previously studied computationally by utilizing advanced ab initio methods describing the characteristic biradicaloid properties of these compounds.[4, 46-48] The *cis* isomer (Figure 2b) shows a greater biradical character as a result of meta (*cis*) and para (*trans*) quinodimethane moieties, affecting the number of Clar's sextets in the covalent and biradical valence bond structure.[49] As demonstrated in Figure 2, two Clar's sextet appear in the Kekulé structure of the *trans*-isomer (Figure 2a) and only one appears in that of the *cis*-isomer (Figure 2b), while three Clar's sextet appear for the biradical form of both the isomers. Therefore, in the *cis*-isomer, the relative weight of the biradical form is greater than that of the *trans*-isomer due to the difference in quinoid valence bond structures.[50-52] The strongly enhanced biradical character of the *cis*-isomers has been shown also by Fukuda et al.[50] and by MR-AQCC calculations.[4]

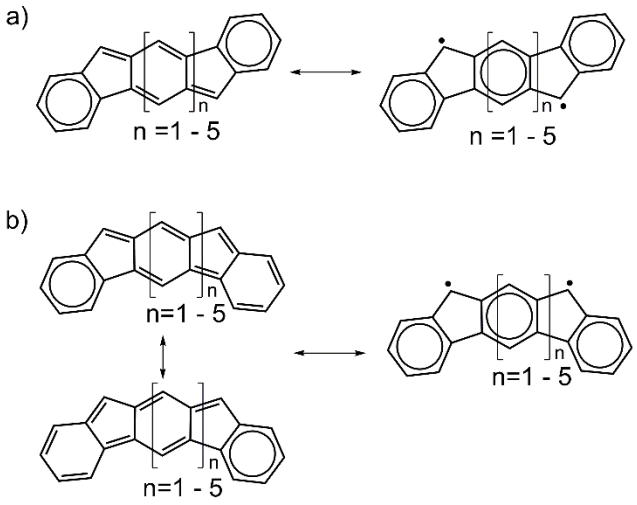

Figure 2. Structures of a) *trans*-diindenoacenes (**5-9**) and b) *cis*-diindenoacenes (**10-14**) showing quinoid Kekulé (left) and biradical (right) resonance structures. The circles indicate Clar's aromatic sextet rings.

Zethrenes (Figure 3, structures **15-19**) are z-shaped hydrocarbons with quinoidal and diradical resonance forms.[25] The fusion of two benzenoid rings on the heptazethrene core form 1,2:9,10-dibenzozethrene (structure **15**, Figure 3, Figure 4a) and shows three Clar's sextets in the open-shell biradical resonance valence bond structures in Figure 4b,c. The theoretical study of different zethrenes by variation of the connectivity of the phenylalanyl moieties (a compound

which will further discussed below) lead to planar **15-17** and non-planar **18-19** cethrenes (Figure 3) and are of interest from the viewpoint of better understanding the open shell character of these systems. In **18**, the presence of a sp^3 hybridized carbon leads to non-planarity as the two neighboring hydrogens are above and below the plane, respectively.[53] In **19**, the structure is twisted.

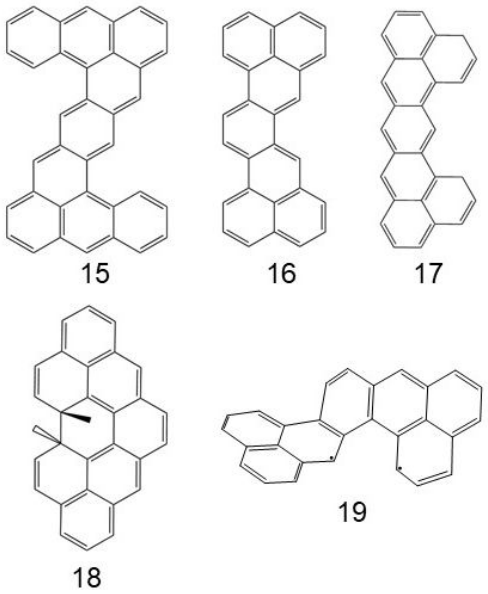

Figure 3. Structures of planar (**15-17**) and nonplanar cethrenes (**18-19**).

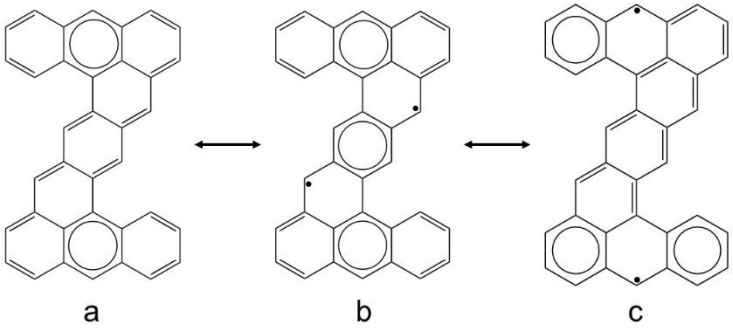

Figure 4: VB structures of 1-2;9,10-Dibenzoheptazethrene (**15**) showing quinoid Kekulé and biradical resonance forms. The circles represent Clar's aromatic sextet rings.

Phenalenyl[5, 54] (**20**) is a rigid π-conjugated neutral radical constructed by triangular fusion of three benzene rings, making phenalenyl the smallest open-shell graphene fragment (see Figure 5 for this and the structures of the following compounds discussed in this paragraph). The

circular extension of phenalenyl with benzene rings leads to several π-conjugated phenalenyl derivatives like biradical triangulene[55-57] (**21**). Further substitution of triangulene with heteroatoms like oxygen (**22**) and phenyl groups (**23**) are shown in Figure 5. Doubly benzylic radicals like fluorenyl (**24)** are π radicals where the radical character can delocalize into neighboring aromatic rings. Fluoranthene (**25**) with a five membered central ring connecting a naphthalene and a benzene unit is a structural isomer of pyrene. The extended fluroanthene structure incorporating another fused naphthalene substructure, acenaphtho[1,2-k]fluoranthene **26,** is an aromatic PAH.[58, 59] A PAH formed by substituting phenyl rings by CH_2 (**27**) in the Chichibabin's hydrocarbon[60] has an open shell radical character. Another example of a molecule with radical character is the quinodimethane derivative 2,6-anthraquinodimethane, **28**. The quinoid Kekulé and biradical resonance structures are shown in Figure 6. Bis-periazulene, **29,** an isomer of pyrene also shows some interesting electronic features[61] such as a peripherally delocalized 14- π system.[62]

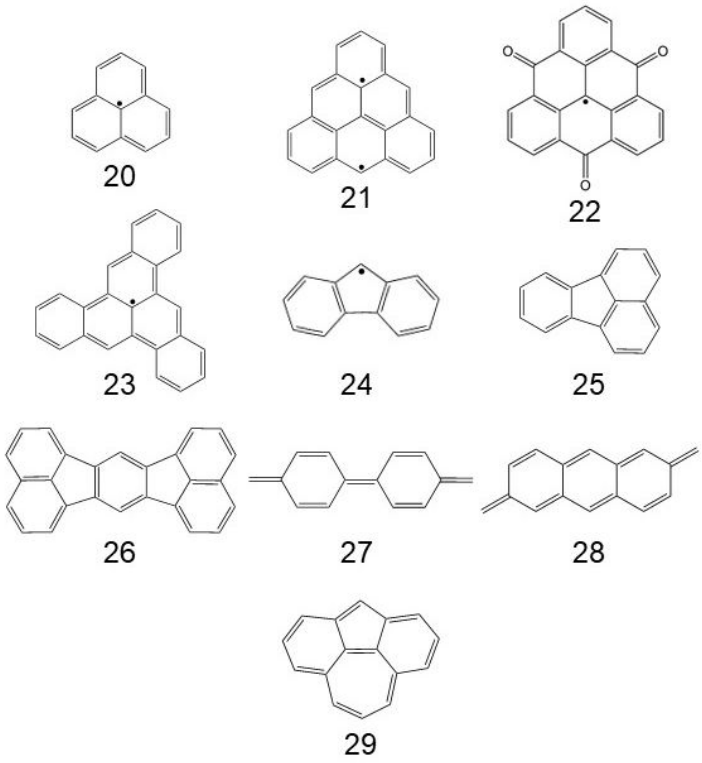

Figure 5. Structures of phenalenyl (PLY) (**20**), triangulene (6TRI) (**21**), O-substituted triangulene (R3-6TRI) (**22**), phenyl-substituted phenalenyl (3P-PLY) (**23**), fluorenyl (**24**), fluoroanthene (**25**), acenaphthylene (**26**), CH_2-terminated Chichibabin's hydrocarbon (**27**), 2,6-anthraquinodimethane (**28**), bis-periazulene (**29**).

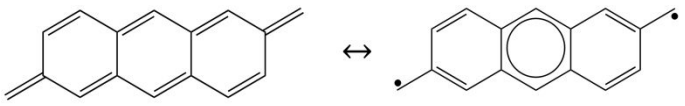

Figure 6. Structure of 2,6-anthraquinodimethane (**28**) showing quinoid Kekulé and biradical resonance forms. The circle represent Clar's aromatic sextet ring.

3. COMPUTATIONAL DETAILS

The polyradical character of the compounds **1-29** were investigated using the MR-AQCC[24] as standard approach and MR-configuration interaction with singles and doubles (CISD)[23] methods in special cases. Size-extensivity corrections are added to the MR-CISD energy (indicated by the symbol +Q) using the Pople correction.[23, 63, 64] The choice of these reference spaces has been made based on the weight of the reference configurations in the wavefunction expansion (non-reference configurations should have a weight <2%), on NO occupations, and experience obtained with previous calculations on the typical biradical compound heptazethrene.[65] The orbitals for MR-CISD+Q and MR-AQCC calculations were computed at the CASSCF level averaging over two states (SA2), the lowest singlet and triplet states or doublet and quartet states depending on the case. These calculations were carried out utilizing CAS(8,8) reference spaces to calculate the lowest singlet/triplet states of molecules with even numbers of electrons. Intruder states (configurations with >2% weight not belonging to the reference space) were corrected at the MR-AQCC level for structures **1-3**, **5**, **12**, **14**, **17-18**, and **29** by including the respective electron configurations into the reference space for both multiplicities. MR-CISD+Q calculations were performed utilizing a CAS(8,8) reference space to calculate the lowest singlet/triplet states of **16** and **26**. The reason for using MR-CISD+Q instead of the standard MR-AQCC was the occurrence of persistent intruder states in the MR-AQCC calculations for the triplet states of **16** and **26**. Respective results are labeled accordingly in the discussion of results below. It has also been shown that for the calculation of energy differences between same or different spin multiplicities for phenalenyl, freezing of all σ orbitals influenced the results by ~0.1 eV only.[25] Reducing the basis set size to 6-31G*[66] had a minor effect on the energy splitting as well. Thus, for all planar structures, the σ orbitals (both occupied and virtual) were kept frozen in all CASSCF, MR-CISD and MR-AQCC calculations at the initial SCF level

while all π orbitals were included. The 6-311G* basis set[67, 68] was used for MR-AQCC and MR-CISD calculations for all the compounds except **18-19** (non-planar cethrenes). To reduce the strongly increased computer times in these non-planar structures, the calculations were performed with the 6-31G basis set and using localized molecular orbitals (MOs) for reference doubly occupied orbitals in the framework of the weak pairs approximation as described in Refs. [69] and [65]. The localized valence σ orbitals were frozen at the MR-AQCC level. In these calculations, the default value of 1.0 was chosen for the radius multiplier, a choice which left the singlet/triplet energies for zethrenes practically unchanged relative to the full calculation as reported in in Ref. [65].

The ground states of all structures utilized for MR-AQCC and MR-CISD calculations were optimized at DFT level using the TPSS density functional[70] and the def2-TZVP[71, 72] basis set. It should be noted that these calculations were performed without dispersion correction. Test calculations showed that the effect on the PAH geometries is very small and did not affect the analysis of their biradical character. Table S1 shows for four test examples chosen from each of the four PAH groups an average RMSD difference of 0.004 Å between structures with/without D3. These small differences do not affect our FOD analysis and the comparison with unpaired density values. In case of the DFT calculations, the low-spin ground state electron configuration was determined by wave function instability analysis[73] of the Kohn-Sham determinants.[74] The compounds **3-4**, **8-17**, and **19** were found to have triplet instabilities present in their wave functions at restricted DFT (RDFT) level, which were reoptimized using an unrestricted DFT (UDFT) approach. The harmonic vibrational frequencies for all structures were calculated using the same functionals and basis sets as for the respective geometry optimizations and found to be positive in all cases, exceptions for the 1 ^1A_g state of compounds **15** which shows an out-of-plane imaginary frequency in C_{2h} symmetry as discussed in previous work.[25] Compound **27** also showed a minor degree of out-of-plane character. For the sake of computational efficiency, these smaller violations of planarity were ignored, and the higher symmetry was kept in these two cases.

The singlet/triplet splitting energy ($\Delta E_{S\text{-}T}$) is calculated by subtracting E_S from E_T, such that positive values mean that the low spin state is the ground state. The total number of unpaired electrons (N_U) and the unpaired electron density[32, 75] were calculated using Eqn. (2) by means of the non-linear formula developed by Head-Gordon[31] where the sum is taken over all NOs:

$$N_U = \sum_{i=1}^{m} n_i^2 \left(2 - n_i\right)^2 \qquad (2)$$

where n_i is the occupation of the ith NO. For structures with doublet or triplet ground states, values of 1 and 2, respectively are subtracted from the N_U value to give the reduced $N_{U,red.}$. $N_{U(H-L)}$ values are computed by restricting the sum in Eq. (2) to the HONO-LUNO pair.

The FOD analysis has been performed by means of a finite temperature (FT)-DFT approach to obtain the static electron correlation (SEC) based on a pre-defined electronic temperature. The FOD is derived from Eqn. (3) as described in Ref. [33]:

$$\rho^{FOD}\left(r\right) = \sum_{i=1}^{N} \left(\delta_1 - \delta_2 f_i\right) |\varphi_i\left(r\right)|^2 \qquad (3)$$

where the f_i values are the fractional occupation (FO) numbers ($0 \leq f_i \leq 1$) and the sum is taken over all molecular spin orbitals. In Eqn. (3) the constants δ_1 and δ_2 are chosen to be unity if the energy level is lower than the Fermi energy (E_F) while they are zero and -1, respectively, for an energy higher than E_F. The integration of the FOD over all space yields the N_{FOD} value which can be used to quantify the SEC. The FO numbers are obtained from the Fermi-Dirac distribution (Eqn. (4)) depending on the difference of the orbital energy (ε_i) and E_F.

$$f_i = \frac{1}{\varepsilon^{\left(\varepsilon_i - E_F\right)/kT_{el}} + 1} \qquad (4)$$

For open shell cases, the f_i values of a given orbital are summed over the alpha and beta shell contributions. For the cases of doublet or triplet state structures with FT-UDFT, values of 1 or 2 are subtracted from the N_{FOD} resulting in a reduced value, $N_{FOD,red.}$. The recommended choice of the electronic temperature (T_{el}) is established by the empirical formula:

$$T_{el} = 20000K \times a_x + 5000K \qquad (5)$$

where a_x is the amount of non-local Fock exchange admixture in the chosen (hybrid) density functional.[34, 76] These literature-recommended FTs will be distinguished from those that provide improved N_{FOD} values in the present data by adjustment of the FTs. They will be referred to as "improved-present" FT values.

Both FT-RDFT and FT-UDFT calculations are performed and f_i and FOD values are compared. In case a triplet instability was found, an FT-UDFT calculation was performed. For the FOD analysis, the functionals TPSS ($a_x = 0$), B3LYP[77, 78] ($a_x = 0.2$) and M05-2X ($a_x = 0.56$)[79] have been used together with the def2-TZVP basis set. The choice of the M05-X functional is

motivated by its good performance in the validation process of pancake bonded PAH dimer systems, especially for the phenalenyl dimer in comparison of a wide range of other functionals.[80] The a_x values show a wide range of Fock exchange ranging from zero to 56 %. Initially, the following FTs recommended in Ref. 33 (Eqn. (5)) were used for each density functional amounting to the values of 5000 (TPSS), 9000 (B3LYP), and 16200 (M05-2X) K, respectively.

The spin-projected unrestricted Hartree-Fock (UHF) theory was used for analyzing the diradical character y_i (I = 0 or 1) of all structures; the y-values are given by:[20]

$$y_i = 1 - \frac{4\left(n_{HONO-i} - n_{LUNO+i}\right)}{4 + \left(n_{HONO-1} - n_{LUNO+i}\right)^2} \qquad (6)$$

where n_{HONO-i} and n_{LUNO+i} are the occupation numbers of the ith highest occupied NO (HONO) and the ith lowest occupied NO (LUNO) computed from UHF NOs. A pure closed-shell system has $y_0 = 0$, while a perfect diradical system has $y_0 = 1$ and $y_1 = 0$. In comparison of y_0 with N_U values, the former will be multiplied by a factor of two to achieve consistent counting of electrons.

When calculating the $\Delta E_{S\text{-}T}$ for the singlet ground state structures, UDFT results will be utilized for those cases with triplet instabilities, but RDFT will be used for those cases that are triplet stable. When presenting the N_{FOD} and f_i results in the main text, FT-RDFT results will be given for all structures with singlet ground electronic states even when triplet unstable. The remaining FT-UDFT results will be presented in the Supplementary Information (SI) and discussed in the main text in the appropriate context. It is often the case that the FT-UDFT results will be the same as the FT-RDFT results despite beginning from a triplet unstable calculation. Regardless, both sets of data are presented.

The geometry optimizations, stability analysis, and frequency calculations were carried out using the Gaussian program package.[81] All CASSCF, MR-CISD and MR-AQCC calculations were performed using the COLUMBUS 7.2 program suite.[82, 83] The unpaired electron population analysis and N_U values were calculated using the TheoDORE 3.0 program.[84-86] The FT-DFT and $\Delta E_{S\text{-}T}$ calculations were carried out with the Turbomole 7.5 program.[87] The FOD analysis for FT-DFT calculation was done using the foden/Turbomole program.[33]

4. RESULTS AND DISCUSSION

4.1. Properties of Benchmark Compounds

4.1.1. *n*-Acenes

The polyradicaloid character of quasi one-dimensional *n*-acenes have been investigated extensively before at MR-AQCC level.[7] A selection of them (*n* = 4, 6,8 and 10, **1-4,** Figure 1) is being used here for benchmarking the DFT functionals selected in this work. To start with, Table 1 lists the vertical singlet/triplet splitting energy, $\Delta E_{S\text{-}T}$, calculated with the MR-AQCC and the different DFT methods. For all methods, the $\Delta E_{S\text{-}T}$ decreases as the length of the chain increases indicating an increasing multiradical character. $\Delta E_{S\text{-}T}$ shows a steep decrease from **1** to **2** as the energy decreases from 41.1 kcal/mol to 25.7 kcal/mol (MR-AQCC), then follows a more gradual decrease from **2** to **3** as given in Table 1. The $\Delta E_{S\text{-}T}$ for **4** decreases to 7.9 kcal/mol. These results agree well with previous MR-AQCC calculations using a CAS(8,8) reference and the smaller 6-31G basis.[88] The trends in the corresponding DFT results compare quite well to MR-AQCC data. The absolute values of singlet/triplet splitting agree also well for structure **1** (tetracene) among all methods. For the larger acenes, the decrease of the $\Delta E_{S\text{-}T}$ values differs somewhat for the different methods. TPSS gives the smallest splitting for structure 4 (tetracene).

Table 1. Vertical singlet/triplet splitting energy ($\Delta E_{S\text{-}T}$, $E(1^3B_{1u}) - E(1^1A_g)$) in kcal/mol calculated at the MR-AQCC level and using different DFT functionals for the *n*-acenes (**1-4**).[a]

Structure	MR-AQCC	M05-2X	TPSS	B3LYP
1	41.0	36.2	30.4	32.5
2	25.7	16.8	12.3	14.0
3	18.0	11.2	4.1	7.1
4	7.9	10.0	2.4	5.2

[a] The following structures are triplet stable at the RDFT level: M05-2X: **1**, TPSS: **1-2**, and B3LYP: **1**. The remaining structures are triplet unstable and derived from UDFT calculations.

NO occupations and N_U values for MR-AQCC calculations for the singlet ground state of **1-4** are given in Table 2. The N_U values increase as the chain length increases from **1** to **4**. The near closed shell character of **1** is seen from a lower N_U value and HONO/LUNO occupation numbers not deviating much from the limiting values of zero/two. As the chain length increases, the open shell character increases showing larger deviations from the closed-shell reference values of zero/two. **4** has the highest N_U value (3.66 *e*) in this series. The N_{FOD} values obtained from M05-2X FT-DFT calculations follow the same trend as the N_U values (Table 2). FT-RDFT

results are the same as FT-UDFT results (Table S2 of the Supplementary Information (SI)) in all cases showing how the finite temperature calculation counteracts the breaking of the spin symmetry. As discussed further below, by comparison to the AQCC NO occupations and N_U values, systematic improvements can be made to the FT-DFT results (N_{FOD} and f_i values) by adjusting the originally recommended FTs. Further justification for this improvement in temperature will be discussed later, and only a description of the relevant results will be presented here. When using the improved-present FTs, the N_{FOD} values agree much better with N_U values as can be seen for M05-2X in Table 2, italicized values), and for TPSS and B3LYP in Tables S2 and S3, italicized values.

Utilizing the default temperature for the M05-2X calculations overestimates the N_{FOD} values considerably compared to the AQCC N_U values (Table 2). For TPSS (Table S3, default temperatures), except for **1** and **4**, the FT-RDFT N_{FOD} values are larger than their respective N_U values. Where applicable, FT-UDFT N_{FOD} values (Table S2) are the same as the FT-RDFT results. With B3LYP, (Table S3, default temperatures), the differences between N_U and N_{FOD} values are similar compared to the other two functionals and are reduced by the improved-present temperature. The trend in the FT orbital occupations f_i (Table 2 and Table S3) reflect the increasing open shell character of the acenes in the same way as the NO occupations.

Table 2. HONO-LUNO occupations and N_U values (MR-AQCC), HOMO-LUMO f_i and N_{FOD} values (M05-2X with FT-RDFT approach) for the *n*-acenes (**1-4**). FT-DFT calculations performed with the literature-recommended temperature (16200 K) and improved-present temperature (12200 K, values in italics). All values are given in units of *e*.

Str		MR-AQCC		FT-RDFT/FOD			
		NO Occ.	N_U	f_i values		N_{FOD}	
1	H	1.80	0.61	1.54	*1.73*	1.81	*0.80*
	L	0.20		0.42	*0.26*		
2	H	1.70	1.13	1.32	*1.51*	2.96	*1.55*
	L	0.30		0.65	*0.50*		
3	H	1.54	1.97	1.18	*1.32*	4.14	*2.36*
	L	0.45		0.80	*0.70*		
4	H	1.12	3.66	1.02	*1.09*	5.49	*3.43*
	L	0.88		0.97	*0.95*		

A plot of f_i values versus MR-AQCC NO occupations for **1-4** is shown in Figure 7 for the improved-present FT of 12200 K for M05-2X showing similar trends in both cases for increasing

acene chain length. Somewhat stronger deviations from the MR-AQCC NOs occupations are observed for the literature-recommended FT (Figure S1, 16200 K).

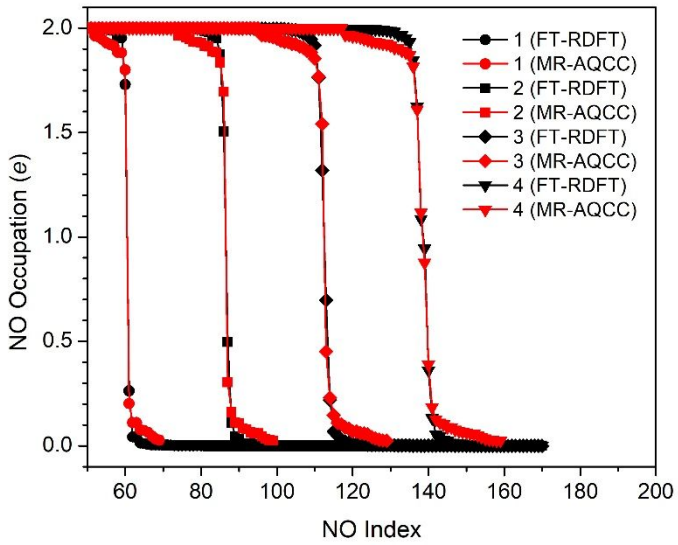

Figure 7. Comparison between FT-RDFT/M05-2X f_i occupation and MR-AQCC NO occupation for the *n*-acenes (**1-4**). FT-RDFT calculations performed at the improved-present FT of 12200 K.

Plots of total unpaired electron density from MR-AQCC and FOD (TPSS density functional) are compared in Figure 8 for **3** (8-acene).The electron density is concentrated on carbon atoms situated on the edges of the chain for both MR-AQCC (Figure 8a) and FOD (Figure 8b). The unpaired density and FOD plots of the remaining structures **1**, **2**, and **4** are presented in Figure S2.

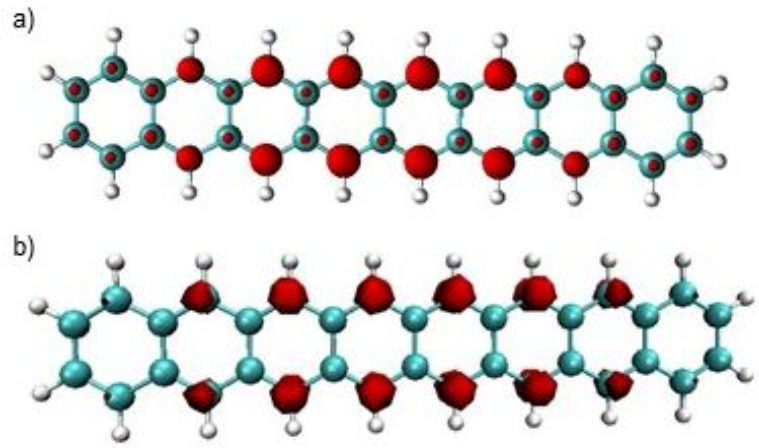

Figure 8. Plots of 8-acene (**3**) showing a) for MR-AQCC unpaired density and b) the corresponding FT-DFT FOD (TPSS density functional, literature-recommended temperature, 5000 K). The isovalue is 0.004 e/bohr^3

4.1.2. Diindenoacene Isomers

Vertical singlet/triplet splitting energies, ΔE_{S-T}, calculated at the MR-AQCC level, are given in Table 3 for *trans*-diindenoacenes (**5-9**) and *cis*-diindenoacenes (**10-14**). The ΔE_{S-T} values decrease as the number of benzene rings *n* of the internal acene chain increases. Initially, the ΔE_{S-T} value decreases steeply in comparison to the subsequent reductions. In comparison to *trans*-diindenoacenes, the *cis*-isomers **10-14** show significantly enhanced open shell character[4, 50] which can be seen from the much smaller ΔE_{S-T} values. A more extended analysis of these structures can be found in previous work.[4] The negative ΔE_{S-T} for **12**, **13**, and **14** shows the triplet state slightly more stable than the singlet state. In general, the DFT calculations (Table 3) give similar ΔE_{S-T} values compared to MR-AQCC. It should be noted that TPSS gives positive ΔE_{S-T} values meaning that the singlet state is the lower one.

Table 3: Vertical singlet/triplet splitting energy (ΔE_{S-T}, $E(1^3B_u)$ - $E(1^1A_g)$ for *trans*-diindenoacenes **5-9** and ΔE_{S-T}, $E(1^3B_1)$ - $E(1^1A_1)$) (kcal/mol) for *cis*-diindenoacenes **10-14** calculated using MR-AQCC/6-311G* and different DFT functionals.[a]

Structure	MR-AQCC	M05-2X	TPSS	B3LYP
5	30.8	24.2	25.0	24.5
6	17.1	12.1	15.1	13.0
7	10.8	7.5	9.9	7.9
8	6.7	5.1	6.3	5.1
9	6.6	4.5	4.7	3.9
10	4.9	2.5	5.4	3.8
11	1.9	1.3	4.1	2.5
12	-0.1	0.0	2.5	1.1
13	-1.0	-1.0	1.2	0.0
14	-2.7	-2.1	0.1	-0.9

[a] The following structures are triplet stable at the RDFT level: M05-2X: **5**, TPSS: **5-7**, and B3LYP: **5**. The remaining structures are triplet unstable and derived from UDFT calculations.

N_U values calculated with MR-AQCC and N_{FOD} calculated with restricted FT-RDFT using the M05-2X functional are compared in Table 4 with the literature-recommended FT (non-italicized values). *Trans*-diindenobenzene (**5)** shows quite a low open shell character (N_U =0.71 *e*) as compared to *trans*-diindenopentacene (**9**) (N_U =2.58 *e*). The same pattern is seen for *cis*-

isomers, but the N_U values are significantly larger than those for respective *trans*-diindenoacenes, owing to the enhanced open shell character of *cis*-diindenoacenes. N_{FOD} values computed with M05-2X compare well when utilizing the improved-present FT of 12200 K; those obtained with the literature recommended FT are significantly too large. Likewise, the difference in NO occupations and f_i values are smaller with the improved-present temperature as well. The agreement to HONO/LUNO values is consistently improved by using the improved (smaller) present temperatures. The FT-UDFT results for the M05-2X functional can be found in Table S4. The nice agreement of the trend in NO occupations with FT-RDFT/M05-2X f_i occupation is shown in Figure 9. It is noted that the FT-DFT approach results in equal values for FT-RDFT and FT-UDFT calculations for structures **6-9** and **12-14** even though the respective calculations without FT give different energies. The comparison of N_U and f_i values calculated at the literature-recommended FT is found in Figure S3.

Table 4. HONO-LUNO occupations and N_U values (MR-AQCC/6-311G* method), HOMO-LUMO f_i and N_{FOD} values (M05-2X method with FT-RDFT approach) for *trans*-diindenoacenes (**5-9**) and *cis*-diindenoacenes (**10-14**). FT-DFT calculations performed with the literature-recommended (non-italicized values, 16200 K) and present improved-present temperatures (12200 K, values in italics). All values are given in units of *e*.

Str		MR-AQCC		FT-RDFT/FOD			
		NO Occ.	N_U	f_i values		N_{FOD}	
5	H	1.78	0.71	1.60	*1.74*	2.22	*1.09*
	L	0.24		0.62	*0.41*		
6	H	1.68	1.09	1.44	*1.58*	2.80	*1.51*
	L	0.34		0.73	*0.56*		
7	H	1.56	1.59	1.33	*1.45*	3.36	*1.91*
	L	0.45		0.78	*0.66*		
8	H	1.43	2.15	1.24	*1.33*	3.93	*2.32*
	L	0.58		0.82	*0.73*		
9	H	1.38	2.58	1.18	*1.25*	4.50	*2.71*
	L	0.63		0.84	*0.77*		
10	H	1.56	1.39	1.36	*1.46*	2.68	*1.68*
	L	0.46		0.86	*0.72*		
11	H	1.43	1.89	1.29	*1.38*	3.10	*1.94*
	L	0.59		0.88	*0.77*		
12	H	1.31	2.14	1.22	*1.28*	3.59	*2.25*
	L	0.69		0.89	*0.82*		
13	H	1.21	2.68	1.15	*1.20*	4.11	*2.58*
	L	0.80		0.90	*0.85*		
14	H	1.16	2.91	1.10	*1.14*	4.65	*2.93*

L	0.83	0.91	*0.87*

The FT-DFT results utilizing the TPSS and B3LYP functionals are collected in Table S4 (FT-UDFT) and Table S5 (FT-RDFT) for comparison. When utilizing the improved-present FT with TPSS (6200 K), the largest difference is the N_{FOD} value for structure **5** (+0.41 *e* compared to N_U); the other N_{FOD} values are within +0.30 *e* of their respective N_U values. For B3LYP and using the improved-present FT, the differences in N_{FOD} and N_U are the largest again for **5** and **6** (+0.37 *e*), and the remaining structures have N_{FOD} values within ±0.27 *e* or smaller of their respective N_U values.

For TPSS and the literature-recommended FT, the f_i and N_{FOD} values (FT-RDFT) compare qualitatively with the AQCC NO occupations and N_U values, though the former values are smaller in most cases. The differences are largest for N_U and N_{FOD}, while the HONO-LUNO occupations (AQCC) and HOMO-LUMO f_i values (FT-RDFT) compare quite well. This suggests that the contributions of orbitals other than HOMO-LUMO are larger with FT-DFT than with MR-AQCC. FT-RDFT and FT-UDFT agree well for TPSS.

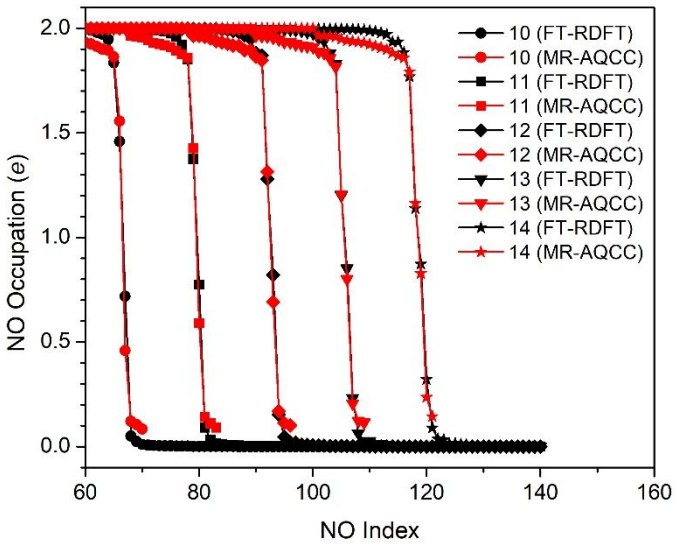

Figure 9. Comparison between FT-RDFT/M05-2X f_i occupation and MR-AQCC NO occupation for all *cis*-diindenoacenes (**10-14**). FT-RDFT calculations performed at the improved-present FT of 12200 K.

The total unpaired electron density plot computed with MR-AQCC is compared to the respective FOD plot using the TPSS functional for the singlet state of *cis*-diindenoanthracene (**12**) in Figure 10. For both methods the electron density is concentrated on the apical carbon atoms of the five-membered rings, in agreement with the biradical VB structure shown in Figure 2. Further unpaired density is distributed in an alternant way primarily into the anthracene segment of the *cis*-diindenoanthracene. Both plots are very similar, differing only in scale due to the larger N_U value of 2.1 *e* as compared to the smaller FOD number of 1.7 *e*. The unpaired density and FOD plots for the remaining structures **5-9** (*trans*-isomers) and **10**, **11**, **13**, and **14** (*cis*-isomers) are presented in Figures S4 and S5, respectively.

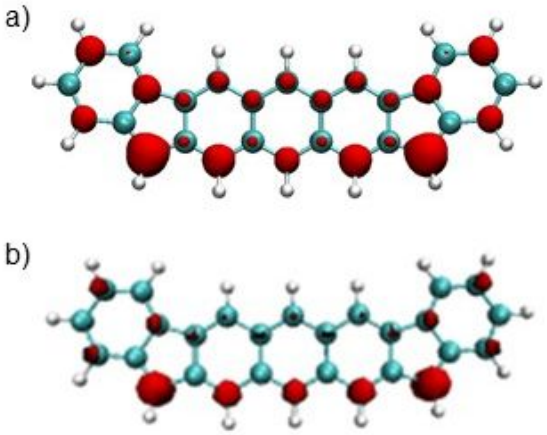

Figure 10. Plots for **12**, *cis*-diindenoanthracene of the a) MR-AQCC unpaired density and b) FT-DFT FOD (TPSS density functional, literature-recommended temperature, 5000 K). The isovalue = 0.004 e/bohr^3.

4.1.3. Zethrenes

The MR-AQCC vertical singlet/triplet splitting, ΔE_{S-T}, for **15**, **17-19**, and MRCISD+Q splittings for **16**, and DFT results are collected in Table 5. Structures **15**, **16** and **18** have singlet ground states whereas **17** and **19** possess triplet ground states. The singlet/triplet splitting energies are relatively small for **15** and **16** (14.0 and 16.5 kcal/mol, respectively). More information on the singlet/triplet splitting energies for planar zethrenes with several multireference schemes and basis sets can be found in previous calculations.[25] Structure **19** is a biradical while **18** possesses a closed shell structure Therefore, the latter has a large singlet-

triplet splitting gap of 52.6 kcal/mol. The different DFT singlet-triplet splittings agree quite well with the MR-AQCC results.

Table 5. Vertical singlet/triplet splitting energy, $\Delta E_{S\text{-}T}$ (kcal/mol) calculated using the MR-AQCC method (**15**, **17-19**), MR-CISD+Q method (**16**, indicated with *),[a] and different DFT functionals for zethrenes (**15-19**).[b] The ground state and excited state is shown for each system.

Str.	MR-AQCC	M05-2X	TPSS	B3LYP
15		$E(1^3B_u) - E(1^1A_g)$		
	14.0	10.6	11.0	9.9
16		$E(^3B_1) - E(^1A_1)$		
	16.5*	7.9	7.5	*7.0*
17		$E(^3B_1) - E(^1A_1)$		
	-11.0	-4.3	-2.3	-3.2
18		$E(1^3A) - E(1^1A)$		
	52.6	61.0	45.0	51.1
19		$E(1^3A) - E(1^1A)$		
	-2.0	-3.8	-2.0	-2.8

[a] MR-CISD+Q calculations were performed in this case because of persistent intruder states encountered in MR-AQCC calculations for the triplet state of **16**.
[b] The following structures are triplet stable at the RDFT level: M05-2X: **18**, TPSS: **15** and **18**, and B3LYP: **18**. The remaining structures are triplet unstable and derived from UDFT calculations.

The zethrene NO occupations and N_U values are collected in Table 6 for MR-AQCC calculations; f_i and FOD numbers are given for M05-2X calculations. Structure **15** shows a large N_U value of 1.64 *e* in accord with Clar's rule since there are three aromatic sextets in the biradical VB structures shown in Figure 4. The N_U values of the triplet ground state structures **17** and **19** are dominated by the two open shell electrons of the triplet state. The remaining open shell character ($N_{U,red.}$) is relatively small. Comparing the MR-AQCC N_U values with FT-DFT with the improved-present FT of 12200 K for M05-2X (Table *6*), generally quite good agreement is found. For structures **15**, **16**, and **18**, the N_{FOD} values are within only about 0.48, 0.19, and 0.35 *e*, respectively, of the N_U values. For **17** and **19**, the difference between N_{FOD} and N_U is somewhat larger (+0.51 and 0.57 *e* respectively). FT-UDFT was utilized for **17** and **19** as they have triplet electronic ground states. The FT-RDFT values equal those calculated with FT-UDFT for structures **15** and **16**. Comparing the MR-AQCC N_U values with FT-DFT N_{FOD} numbers using the literature-recommended FT (16200 K) shows larger deviations. The results using the FT-UDFT approach are found in Table S6.

Table 6. HONO-LUNO occupations and N_U values (MR-AQCC/6-311G* method), HOMO-LUMO f_i and N_{FOD} values using the M05-2X method[b] for the zethrene structures (**15**-**19**). FT-DFT calculations performed with the literature-recommended (non-italicized values, 16200 K) and improved-present temperatures (12200 K, values in italics). The $N_{U,red.}$ and $N_{FOD,red.}$ values are provided in parentheses for structures with triplet ground states (**17** and **19**). All values are given in units of *e*.

Str		MR-AQCC		FT-RDFT/FOD: **15**, **16**, **18** FT-UDFT/FOD: **17**, **19**			
		NO Occ.	N_U ($N_{U,red.}$)	f_i Values		N_{FOD} ($N_{FOD,red.}$)	
15	H	1.61	1.64	1.21	*1.36*	3.94	*2.12*
	L	0.39		0.67	*0.56*		
16	H	1.53	1.64	1.19	*1.33*	3.18	*1.83*
	L	0.47		0.72	*0.62*		
17	H	1.82	2.72 (0.72)	1.73	*1.86*	4.92 (2.92)	*3.23 (1.23)*
	S1	1.00		0.99	*1.01*		
	S2	1.00		0.94	*0.96*		
	L	0.18		0.26	*0.14*		
18	H	1.84	0.70	1.63	*1.80*	2.55	*1.05*
	L	0.16		0.32	*0.18*		
19	H	1.84	2.74 (0.74)	1.79	*1.89*	4.88 (2.88)	*3.31 (1.31)*
	S1	1.00		0.97	*0.99*		
	S2	1.00		0.96	*0.98*		
	L	0.15		0.20	*0.11*		

[a] The FT-UDFT approach was utilized for zethrenes **17** and **19** as they have triplet electronic ground states, and the FT-RDFT approach was used for **15**, **16**, and **18**.

Using the TPSS functional and taking the improved-present FT of 6200 K for TPSS (Table S7, italicized values) increases the N_{FOD} values in all cases with FT-RDFT. The FOD values become slightly overestimated compared to the MR-AQCC N_U values in all cases. When considering the improved-present FT of 8200 K with B3LYP, the associated decrease in N_{FOD} values improves the agreement with N_U. As found with the other cases described above, the agreement of the N_U and N_{FOD} at the literature-recommended FT is worse.

Plots of the total unpaired electron density for **16** and **19** with MR-AQCC, respectively, are shown in Figure 11a,c in comparison with respective FOD plots (TPSS density functional) in Figure 11b,d. As in the other cases, FOD provides a good representation of the unpaired density plots. The unpaired density and FOD plots for the remaining structures **15**, **17**, and **18** are presented in Figure S6.

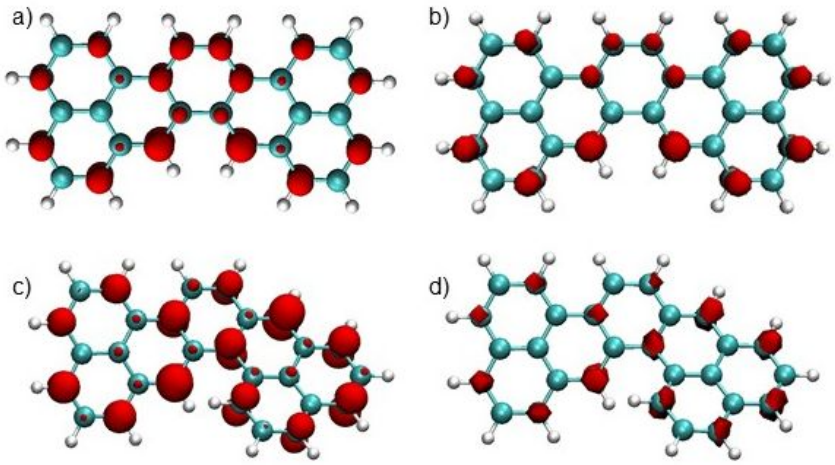

Figure 11. Total MR-AQCC unpaired density plots for a) **16** and c) **19**, respectively, and the corresponding FT-DFT FOD (TPSS density functional, literature-recommended temperature, 5000 K) for b) **16** and d) **19**. The isovalue = 0.004 *e*/bohr^3

4.1.4. Phenalenyl Based Triangular Radicals and Other Compounds

A selection of PAHs (**20-29**, Figure 5) included in this category are studied in analogy to compounds described in the above sections. The MR-AQCC singlet/triplet splitting energies for the structures **25, 27-29** with even number of electrons are collected in Table 7. MR-CISD+Q was utilized for **26** because of persistent intruder states in the triplet state when using the AQCC method. The ΔE_{S-T} is quite large for structures **25** and **26** (60.7 and 67.3 kcal/mol, respectively). Structures **27** and **28** have smaller ΔE_{S-T} values of 20.4 and 22.6 kcal/mol, respectively. For comparison, the ΔE_{S-T} values computed with the three DFT functionals are also presented in Table 7. They are quite close to the MR values, within about 3-8 kcal/mol in most cases.

Table 7. Vertical singlet/triplet splitting energy, ΔE_{S-T} for **25, 27-29** calculated using the MR-AQCC/6-311G* method and the MR-CISD+Q/6-311G* method for **26**[a] (indicated with *)[a] and comparison with different DFT results.[b] The ground state and excited state are shown for each system.

Str	MR-AQCC or MRCISD+Q*	M05-2X	TPSS	B3LYP
25		$E(1^3A_1) - E(1^1A_1)$		
	60.7	66.2	56.8	59.9
26		$E(1^3B_{2u}) - E(1^1A_g)$		
	67.3*	66.7	48.5	54.8
27		$E(1^3B_{1u}) - E(1^1A_g)$		

	20.4	15.1	17.2	15.8
28	$E(1^3B_u) - E(1^1A_g)$			
	22.6	15.6	16.6	15.5
29	$E(1^3B_2) - E(1^1A_1)$			
	11.5	3.3	6.8	5.5

[a] MR-CISD+Q calculations were performed in these cases because of persistent intruder states encountered in MR-AQCC calculations for the triplet state (**26**).
[b] The following structures are triplet stable at the RDFT level: M05-2X: **25**, **26**, **29**, TPSS: **25-29**, and B3LYP: **25**, **26**, **29**. The remaining structures are triplet unstable and derived from UDFT calculations.

The MR-AQCC N_U values are given in Table 8. The N_U values for singlet state structures **27** and **28** are quite large, showing significant biradical character. When calculating the N_{FOD} values with the improved-present FT for the M05-2X functional, good agreement is found in most cases with the N_U values. On the other hand, the literature-recommended FT (12600 K) again overestimates the N_{FOD} values. Similarly good agreement is found for TPSS and B3LYP (Table S8) as well when using the improved-present FT (6200 and 8200 K, respectively), and compare better to N_U than those calculated with the literature-recommended FTs. FT-UDFT values are given for comparison in Table S9. For structure **27**, the FT-UDFT values are the same as those calculated with FT-RDFT. FT-UDFT was utilized for structures **20-24** as they have either doublet or triplet electronic ground states.

Table 8. HONO-LUNO occupations and N_U values (MR-AQCC/6-311G* method), HOMO-LUMO f_i and N_{FOD} values using the M05-2X method[b] for compounds **20-29**. FT-DFT calculations performed with the literature-recommended (non-italicized values, 16200 K) and improved-present temperatures (12200 K, values italics). The $N_{U,red.}$ and $N_{FOD,red.}$ values are provided in parentheses for structures with doublet or triplet ground states (**20-24**). All values are given in units of *e*.

Str		MR-AQCC		FT-RDFT/FOD: **25-29** FT-UDFT/FOD: **20-24**			
		NO Occ.	N_U ($N_{U,red.}$)	f_i Values		N_{FOD} ($N_{FOD,red.}$)	
20	H	1.87	1.35 (0.35)	1.89	*1.95*	2.29 (1.29)	*1.62 (0.62)*
	S1	1.00		0.96	*0.98*		
	L	0.12		0.11	*0.06*		
21	H	1.87	2.50 (0.50)	1.85	*1.93*	4.21 (2.21)	*2.96 (0.96)*
	S1	1.00		0.99	*1.00*		
	S2	1.00		0.99	*1.00*		
	L	0.13		0.14	*0.07*		
22	H	1.88	1.57	1.87	*1.94*	3.56	*2.12*

	S1	1.01	(0.57)	1.21	*1.12*	(2.56)	*(1.12)*
	L	0.13		0.25	*0.11*		
23	H	1.86	1.61 (0.61)	1.79	*1.89*	3.50 (2.50)	*2.17 (1.17)*
	S1	1.00		0.95	*0.96*		
	L	0.14		0.21	*0.11*		
24	H	1.88	1.32 (0.32)	1.76	*1.86*	2.36 (1.36)	*1.61 (0.61)*
	S1	1.01		1.11	*1.09*		
	L	0.12		0.15	*0.07*		
25	H	1.86	0.36	1.78	*1.90*	1.37	*0.52*
	L	0.13		0.30	*0.16*		
26	H	1.86	0.64	1.72	*1.86*	2.33	*0.95*
	L	0.15		0.40	*0.23*		
27	H	1.66	0.95	1.42	*1.61*	1.78	*0.94*
	L	0.34		0.53	*0.38*		
28	H	1.67	0.99	1.43	*1.61*	2.04	*1.07*
	L	0.33		0.54	*0.38*		
29	H	1.79	0.75	1.33	*1.47*	2.24	*1.37*
	L	0.21		0.66	*0.53*		

[a] The FT-UDFT approach for **20**-**24** as they have doublet or triplet ground electronic states and the FT-RDFT approach for **25**-**29**.

Unpaired and FOD densities, respectively, are shown in Figure 12 for **28** and **29.** Figure 12a,b shows the unpaired density and FOD located on the CH_2 group of **28** and on the alternant C atom close to the CH_2 group. The unpaired density and FOD plots for the remaining structures **20**-**27** are presented in Figure S7.

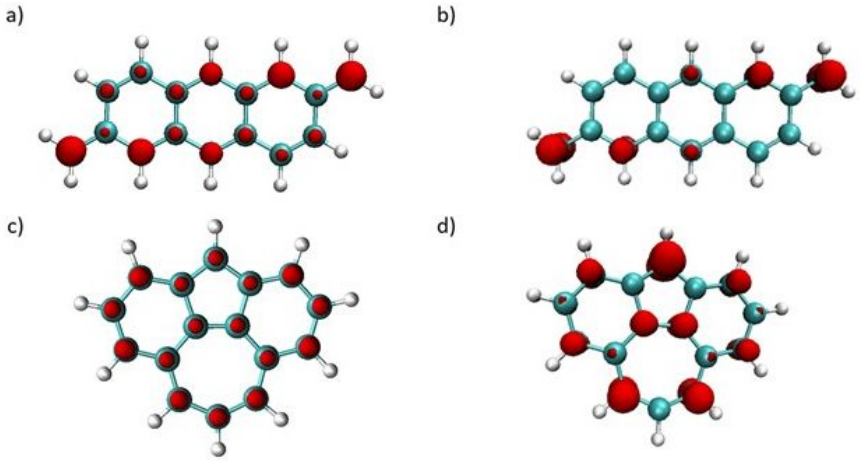

Figure 12. Total MR-AQCC unpaired density plots for a) **28** and c) **29** and the corresponding FT-DFT FOD (TPSS density functional, literature-recommended temperature, 5000 K) for b) **28** and d) **29**. The isovalue = 0.004 e/bohr^3.

4.2. Regression Analysis of Biradical Descriptors in Relation to MR-AQCC N_U Values

In the following analysis, a regression analysis is used to assess the overall agreement between the MR-AQCC N_U and DFT N_{FOD} values. We are regarding the MR-AQCC N_U values as reference data because they are based on calculations which explicitly taking the multireference character of the wavefunction into account. A regression plot of N_{FOD} values calculated from FT-RDFT/M05-2X vs. N_U values for all 22 structures with singlet ground states (**1-16, 18, 25-29**) is shown in Figure 13a using the literature-recommended FT of 16200 K. In this plot, the correlation coefficient (R^2) between the N_U and N_{FOD} values is 0.95. This indicates that despite the already above-discussed overestimation of the individual N_{FOD} values at this temperature, a very high degree of correlation exists between the N_U and N_{FOD} values. Regardless of this large R^2 values, however, the effects of the overestimation of the N_{FOD} values are reflected in the relatively large slope of 1.8. By reducing the temperature in steps of 1000 K to 12200 K (Figure 13b), the R^2 value increases slightly to 0.98. However, the slope is improved significantly to a value of 1.07, which leads to a still greater numerical similarity between N_U and N_{FOD} values. The same plot for the FT-UDFT results (including those FT-RDFT structures for which no triplet stability was present: **1, 5, 18, 25, 26, 29**) is shown in Figure S8 and a comparable quality of the regression analysis is obtained.

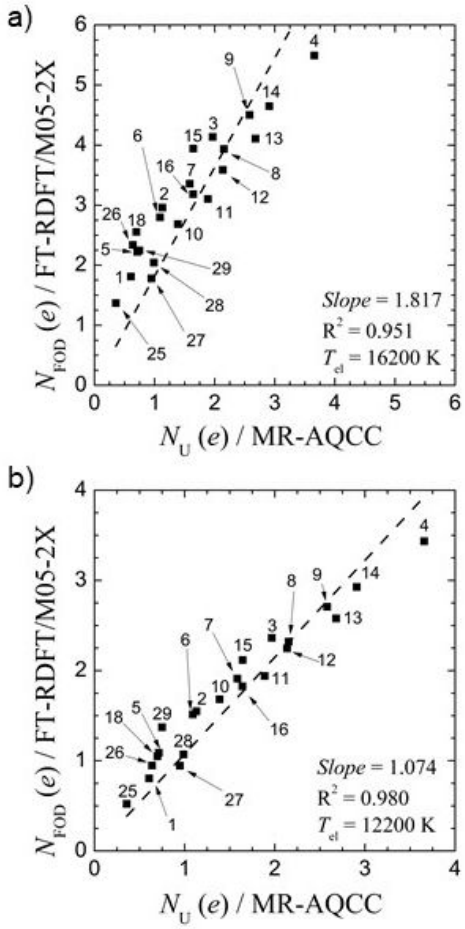

Figure 13: Comparison between MR-AQCC N_U values and FT-RDFT N_{FOD} numbers with the M05-2X density functional for structures with singlet ground electronic state (**1-16, 18, 25-29**) using the a) literature-recommended FT of 16200 K and b) improved-present FT of 12200 K.

When considering the TPSS density functional (Figure S9a), a similar need for rescaling the FT is found. With the literature-recommended FT of 5000 K, we obtained a very good R^2 of 0.98, but the slope of 0.83 is too small. Upon increasing the temperature in steps of 1000 K and refinement with 200 K steps with a final value of 6200 K (Figure S9b), the slope increases to 1.02, while the R^2 value remains practically the same. No correlation diagram with FT-UDFT/TPSS results is shown since in most cases RDFT is stable using TPSS. For B3LYP (Figure S10), the literature-recommended FT of 9000 K results in an R^2 value of 0.97 for FT-RDFT, while the slope is a bit too large. When decreasing the FT in steps of 1000 K and refinement with 200 K steps with a final value of 8200 K (Figure S10c), the slope decreases to 1.03 for FT-RDFT while R^2 remains practically the same, excellent value. In case of UDFT/B3LYP calculations at the original temperature of 9000 K, slope and R^2 turned out to be

very good. Using the optimized temperature of 8200 K for UDFT, showed a slight improvement of the regression quality.

Another popular criterion to analyze the biradical character are the y values (Eqn. (5)) calculated with unrestricted Hartree-Fock (UHF). In Figure 14, y_0 values are compared to N_U values. A very good correlation is found indicated by an R^2 value of 0.96. However, the slope of 1.13 is a little too large. A closely related biradical descriptor is the LUNO occupation. Comparison with N_U has been performed at the UDFT level with the three chosen density functionals for the same set of structures with a singlet ground state as before. However, cases with stable RDFT solution had to be excluded because the LUNO occupation would be zero in this case. For UM05-2X (Figure 15), the R^2 value shows an excellent agreement with N_U, however the slope of 0.31 is quite small. Structure **4** (the largest acene) seems to deviate somewhat more from the trend line than the other structures. Structures **4** and **14** (the largest linear acene and largest cis-diindenoacene, respectively) possess the largest UDFT LUNO occupation. With UTPSS (Figure S11a), the smallest number of structures contribute to the correlation as more of the singlet ground state structures are stable with respect to UDFT. The R^2 value of 0.91 is smaller than that of M05-2X. Remarkably, the slope of 0.19 is very small. For UB3LYP (Figure S11b), the R^2 of 0.97 is larger than that of UTPSS. However, the slope is also very small at 0.25.

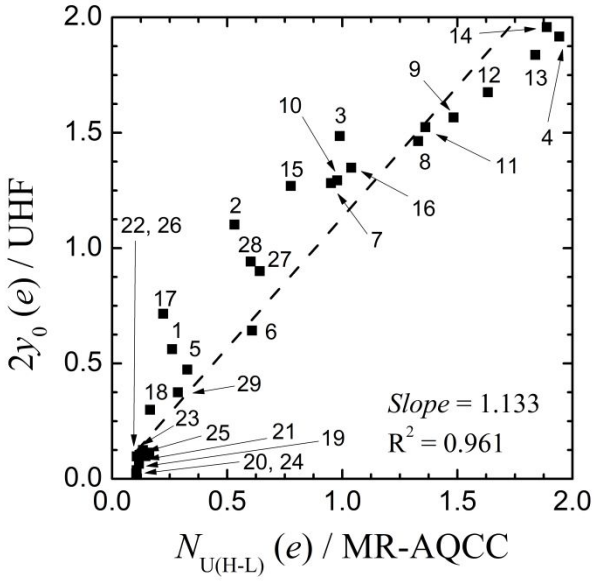

Figure 14. Comparison between the MR-AQCC $N_{U(H-L)}$ with $2y_0$ values for all UHF calculations for molecules with singlet ground electronic states (**1-16, 18, 25-29**).

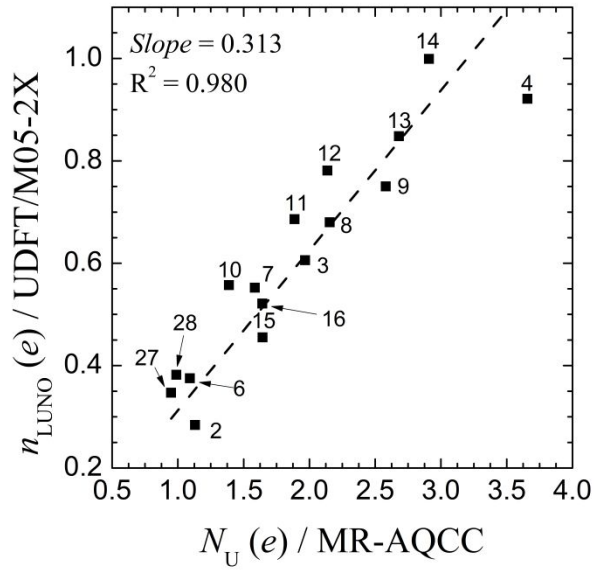

Figure 15. Comparison between the MR-AQCC and UDFT/M05-2X LUNO occupation for all UDFT calculations for molecules with singlet ground states.

The final criterion discussed with respect to description of biradical character is the singlet/triplet splitting energy of the molecules with singlet ground states (**1-16, 18, 25-29**). The

comparison of the MR-AQCC/MR-CISD and M05-2X derived singlet/triplet splitting energies is found in Figure 16. The R^2 values and slope are both close to one at 0.96, indicating excellent agreement between the results obtained with the two methods. When considering the TPSS and B3LYP functionals (Figure S12a,b), the R^2 of the $\Delta E_{S\text{-}T}$ with both functionals quite similar at about 0.96 and 0.97, respectively. The slope is somewhat smaller than one in both cases.

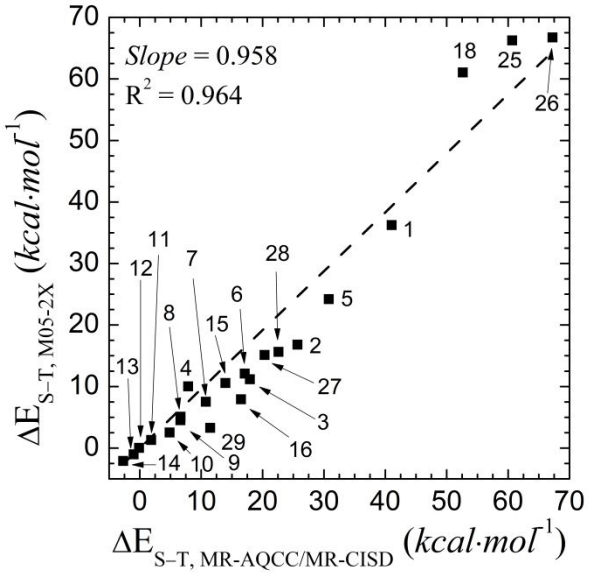

Figure 16. Comparison between the MR-AQCC/MR-CISD+Q and M05-2X singlet/triplet energy ($\Delta E_{S\text{-}T}$) for molecules with singlet ground electronic states (MR-AQCC: **1-15, 18, 25, 27-29**; MR-CISD+Q: **16**, **26**).

Based on the improved-present FTs for the three functionals we determined a new linear regression relation between the non-local Fock exchange and T_{el} in comparison to Eq. (5). It is noted that the regression based on only three functionals is crude, but it still is expected to provide an indication of possible adjustments of the previously suggested relation given in Eq. (5). The linear fit based on the current data is obtained as

$$T_{el} = 10762K \times a_x + 6140K \qquad (7)$$

with an R^2 value of 0.999. This results shows a much smaller slope in comparison to the 20000 K of Eq. (5), but an increased constant value.

5. CONCLUSIONS

MR-AQCC and MR-CISD calculations were carried out to characterize the biradical/radical character of *n*-acenes, diindenoacene isomers**,** zethrenes and various other PAHs by means of $\Delta E_{S\text{-}T}$ values, natural orbital occupations, and unpaired densities. In total 29 compounds were investigated. A detailed comparison with a corresponding FOD analysis based on DFT calculations using three functionals covering a wide range of exact Hartree-Fock exchange was performed. The final good overall statistical correlation between overall biradical descriptors was corroborated by detailed analysis of the evolution of NO occupations (MR-AQCC) with the FT occupation values f_i in series of compounds showing increasing biradical character. Moreover, the FOD plots agreed well with the unpaired densities showing the same electron density distribution patterns, thus allowing a detailed analysis of their atomic localization over the molecules. The FT appeared to be a good and generally well working parameter to achieve a close 1:1 correspondence between MR-AQCC and FOD results after the adjustment of the literature-recommended FT is implemented. It can be noted, however, that the comparison between N_U and N_{FOD} for the radical structures with doublet or triplet ground electronic states **17** and **19-24** is not as good and the N_{FOD} can be larger by about a factor of two in most of these molecules with non-singlet ground states.

The other descriptors considered here, y_0 and n_{LUNO}, showed in part also good correlation with the MR-AQCC N_U values albeit with quite small slopes for the n_{LUNO} descriptor. It appears that there is no general tool available to correct this discrepancy. It should also be noted for these descriptors that even their applicability range depends on the functional used since the DFT triplet stability will vary with the functional used and with it the availability of LUNO occupations.

In summary, the FOD method appears to be a theoretically better founded and more reliable method, which can be well recommended based on the assessment with our MR calculations on PAHs. This finding opens the possibility of large scale and reliable screening of PAH biradical properties, which is expected to have a significant impact on the PAH research field. A new linear fit to our improved-present FTs indicates a much smaller slope in the interpolation line between different non-local Fock exchange percentages, but the fits still show a good linear relationship.

Supplementary Information

Tabulated data of the N_{FOD} and f_i values for the TPSS and B3LYP density functionals. Comparisons of the f_i values and NO occupations for 1-4 and 5-14. Plots of unpaired densities and FOD. Comparison of N_U vs. N_{FOD} for various density functionals. Comparison of N_U vs. n_{LUNO} for TPSS and B3LYP. Comparison of ΔE_{S-T} calculated with FT-DFT and MR-AQCC. Optimized Cartesian coordinates are given.

Acknowledgements

Support by the U.S. National Science Foundation for this research (H.L.: Grant No. CHE-2107923, M.K.: Grant No. CHE-2107820) is gratefully acknowledged. We are grateful for the supply of ample computer time at the HPCC facilities of Texas Tech University.

References

1. A. K. Geim and K. S. Novoselov, *Nat. Mater.*, 2007, **6**, 183-191.
2. B. H. Nguyen and V. H. Nguyen, *Adv. Nat. Sci.: Nanosci. Nanotech.*, 2016, **7**, 023002.
3. Y. Gu, Z. Qiu and K. Müllen, *J. Am. Chem. Soc.*, 2022, **144**, 11499-11524.
4. R. Nieman, N. J. Silva, A. J. A. Aquino, M. M. Haley and H. Lischka, *J. Org. Chem.*, 2020, **85**, 3664-3675.
5. T. Kubo, *Chem. Rec.*, 2015, **15**, 218-232.
6. A. Sánchez-Grande, J. I. Urgel, A. Cahlík, J. Santos, S. Edalatmanesh, E. Rodríguez-Sánchez, K. Lauwaet, P. Mutombo, D. Nachtigallová, R. Nieman, H. Lischka, B. de la Torre, R. Miranda, O. Gröning, N. Martín, P. Jelínek and D. Écija, *Angew. Chem. Int. Ed.*, 2020, **59**, 17594-17599.
7. F. Plasser, H. Pašalić, M. H. Gerzabek, F. Libisch, R. Reiter, J. Burgdörfer, T. Müller, R. Shepard and H. Lischka, *Angew. Chem. Int. Ed.*, 2013, **52**, 2581-2584.
8. H. F. Bettinger, *Pure Appl. Chem.*, 2010, **82**, 905-915.
9. O. Hod, V. Barone and G. E. Scuseria, *Phys. Rev. B*, 2008, **77**, 035411.
10. M. Bendikov, H. M. Duong, K. Starkey, K. N. Houk, E. A. Carter and F. Wudl, *J. Am. Chem. Soc.*, 2004, **126**, 7416-7417.
11. M. Nakano, *SpringerBriefs in Molecular Science: Excitation energies and properties of open-shell singlet molecules. Applications to a new class of molecules for nonlinear optics and singlet fission*, Springer Cham, 2014.
12. T. Minami and M. Nakano, *J. Phys. Chem. Lett.*, 2012, **3**, 145-150.
13. T. D. Nguyen, E. Ehrenfreund and Z. V. Vardeny, *Science*, 2012, **337**, 204-209.
14. J. Wang, A. Chepelianskii, F. Gao and N. C. Greenham, *Nat. Comm.*, 2012, **3**, 1191.
15. Q. Peng, A. Obolda, M. Zhang and F. Li, *Angew. Chem. Int. Ed.*, 2015, **54**, 7091-7095.
16. Y. Morita, S. Nishida, T. Murata, M. Moriguchi, A. Ueda, M. Satoh, K. Arifuku, K. Sato and T. Takui, *Nat. Mater.*, 2011, **10**, 947-951.
17. M. Chikamatsu, T. Mikami, J. Chisaka, Y. Yoshida, R. Azumi, K. Yase, A. Shimizu, T. Kubo, Y. Morita and K. Nakasuji, *Appl. Phys. Lett.*, 2007, **91**, 043506.
18. H. Koike, T. Kubo, K. Uchida, M. Chikamatsu, R. Azumi, K. Mase and K. Kanai, *Appl. Phys. Lett.*, 2013, **102**, 134103.
19. D. Jiang and S. Dai, *J. Phys. Chem. A* 2008, **112**, 332-335.
20. K. Yamaguchi, F. Jensen, A. Dorigo and K. N. Houk, *Chem. Phys. Lett.*, 1988, **149**, 537-542.
21. L. Salem and C. Rowland, *Angew. Chem. Int. Ed.*, 1972, **11**, 92-111.
22. V. Bonačić-Koutecký, J. Koutecký and J. Michl, *Angew. Chem. Int. Ed.*, 1987, **26**, 170-189.
23. P. G. Szalay, T. Müller, G. Gidofalvi, H. Lischka and R. Shepard, *Chem. Rev.*, 2012, **112**, 108-181.
24. P. G. Szalay and R. J. Bartlett, *Chem. Phys. Lett.*, 1993, **214**, 481-488.
25. A. Das, T. Müller, F. Plasser and H. Lischka, *J. Phys. Chem. A* 2016, **120**, 1625-1636.
26. A. Das, M. Pinheiro Jr., F. B. C. Machado, A. J. A. Aquino and H. Lischka, *ChemPhysChem*, 2018, **19**, 2492-2499.
27. K. Yamaguchi, Y. Takahara, T. Fueno and K. N. Houk, *Theor. Chim. Acta*, 1988, **73**, 337-364.

28. D. Doehnert and J. Koutecky, *J. Am. Chem. Soc.*, 1980, **102**, 1789-1796.
29. T. Stuyver, B. Chen, T. Zeng, P. Geerlings, F. De Proft and R. Hoffmann, *Chem. Rev.*, 2019, **119**, 11291-11351.
30. K. Kamada, K. Ohta, A. Shimizu, T. Kubo, R. Kishi, H. Takahashi, E. Botek, B. Champagne and M. Nakano, *J. Phys. Chem. Lett.*, 2010, **1**, 937-940.
31. M. Head-Gordon, *Chem. Phys. Lett.*, 2003, **372**, 508-511.
32. V. N. Staroverov and E. R. Davidson, *Chem. Phys. Lett.*, 2000, **330**, 161-168.
33. S. Grimme and A. Hansen, *Angew. Chem. Int. Ed.*, 2015, **54**, 12308-12313.
34. J.-D. Chai, *J. Chem. Phys.*, 2012, **136**, 154104
35. J.-D. Chai, *J. Chem. Phys.*, 2014, **140**, 18A521.
36. J.-D. Chai, *J. Chem. Phys.*, 2017, **146**, 044102.
37. N. D. Mermin, *Phys. Rev.*, 1965, **137**, A1441-A1443.
38. W. Kohn and L. J. Sham, *Phys. Rev.*, 1965, **140**, A1133-A1138.
39. C. A. Bauer, A. Hansen and S. Grimme, *Chemistry – A European Journal*, 2017, **23**, 6150-6164.
40. F. Liu, C. Duan and H. J. Kulik, *J. Phys. Chem. Lett.*, 2020, **11**, 8067-8076.
41. M. Melle-Franco, *Chem. Commun.*, 2015, **51**, 5387-5390.
42. M. E. Sandoval-Salinas, A. Carreras and D. Casanova, *Phys. Chem. Chem. Phys.*, 2019, **21**, 9069-9076.
43. A. Pérez-Guardiola, M. E. Sandoval-Salinas, D. Casanova, E. San-Fabián, A. J. Pérez-Jiménez and J. C. Sancho-García, *Phys. Chem. Chem. Phys.*, 2018, **20**, 7112-7124.
44. G. E. Rudebusch, J. L. Zafra, K. Jorner, K. Fukuda, J. L. Marshall, I. Arrechea-Marcos, G. L. Espejo, R. Ponce Ortiz, C. J. Gómez-García, L. N. Zakharov, M. Nakano, H. Ottosson, J. Casado and M. M. Haley, *Nature Chem.*, 2016, **8**, 753-759.
45. D. T. Chase, B. D. Rose, S. P. McClintock, L. N. Zakharov and M. M. Haley, *Angew. Chem. Int. Ed.*, 2011, **50**, 1127-1130.
46. D. T. Chase, A. G. Fix, S. J. Kang, B. D. Rose, C. D. Weber, Y. Zhong, L. N. Zakharov, M. C. Lonergan, C. Nuckolls and M. M. Haley, *J. Am. Chem. Soc.*, 2012, **134**, 10349-10352.
47. J.-i. Nishida, H. Deno, S. Ichimura, T. Nakagawa and Y. Yamashita, *J. Mater. Chem.*, 2012, **22**, 4483-4490.
48. J. J. Dressler, M. Teraoka, G. L. Espejo, R. Kishi, S. Takamuku, C. J. Gómez-García, L. N. Zakharov, M. Nakano, J. Casado and M. M. Haley, *Nature Chem.*, 2018, **10**, 1134-1140.
49. A. Shimizu, R. Kishi, M. Nakano, D. Shiomi, K. Sato, T. Takui, I. Hisaki, M. Miyata and Y. Tobe, *Angew. Chem.*, 2013, **125**, 6192-6195.
50. K. Fukuda, T. Nagami, J. Fujiyoshi and M. Nakano, *J. Phys. Chem. A* 2015, **119**, 10620-10627.
51. T. Kubo, *Chem. Lett.*, 2015, **44**, 111-122.
52. M. Abe, *Chem. Rev.*, 2013, **113**, 7011-7088.
53. T. Šolomek, P. Ravat, Z. Mou, M. Kertesz and M. Juríček, *J. Org. Chem.*, 2018, **83**, 4769-4774.
54. Y. Morita, S. Suzuki, K. Sato and T. Takui, *Nature Chem.*, 2011, **3**, 197-204.
55. E. Clar, *Polycyclic hydrocarbons*, Springer, Berlin, Heidelberg, 1964.
56. J. Inoue, K. Fukui, T. Kubo, S. Nakazawa, K. Sato, D. Shiomi, Y. Morita, K. Yamamoto, T. Takui and K. Nakasuji, *J. Am. Chem. Soc.*, 2001, **123**, 12702-12703.

57. K. Fukui, J. Inoue, T. Kubo, S. Nakazawa, T. Aoki, Y. Morita, K. Yamamoto, K. Sato, D. Shiomi, K. Nakasuji and T. Takui, *Synth. Met.*, 2001, **121**, 1824-1825.
58. L. Han, Y. Zhang, W. Chen, X. Cheng, K. Ye, J. Zhang and Y. Wang, *Chem. Commun.*, 2015, **51**, 4477-4480.
59. J. D. Debad and A. J. Bard, *J. Am. Chem. Soc.*, 1998, **120**, 2476-2477.
60. T. Nishiuchi, S. Aibara, H. Sato and T. Kubo, *J. Am. Chem. Soc.*, 2022, **144**, 7479-7488.
61. K. Horii, R. Kishi, M. Nakano, D. Shiomi, K. Sato, T. Takui, A. Konishi and M. Yasuda, *J. Am. Chem. Soc.*, 2022, **144**, 3370-3375.
62. S. Moles Quintero, M. M. Haley, M. Kertesz and J. Casado, *Angew. Chem. Int. Ed.*, 2022, **61**, e202209138.
63. W. L. Luken, *Chem. Phys. Lett.*, 1978, **58**, 421-424.
64. S. R. Langhoff and E. R. Davidson, *Int. J. Quantum Chem.*, 1974, **8**, 61-72.
65. A. Das, T. Müller, F. Plasser, D. B. Krisiloff, E. A. Carter and H. Lischka, *J. Chem. Theory Comput.*, 2017, **13**, 2612-2622.
66. R. Krishnan, J. S. Binkley, R. Seeger and J. A. Pople, *J. Chem. Phys.*, 2008, **72**, 650-654.
67. R. Krishnan, J. S. Binkley, R. Seeger and J. A. Pople, *J. Chem. Phys.*, 1980, **72**, 650-654.
68. A. D. McLean and G. S. Chandler, *J. Chem. Phys.*, 1980, **72**, 5639-5648.
69. D. Walter and E. A. Carter, *Chem. Phys. Lett.*, 2001, **346**, 177-185.
70. J. Tao, J. P. Perdew, V. N. Staroverov and G. E. Scuseria, *Phys. Rev. Lett.*, 2003, **91**, 146401.
71. F. Weigend and R. Ahlrichs, *Phys. Chem. Chem. Phys.*, 2005, **7**, 3297-3305.
72. F. Weigend, *Phys. Chem. Chem. Phys.*, 2006, **8**, 1057-1065.
73. J. Čížek and J. Paldus, *J. Chem. Phys.*, 1967, **47**, 3976-3985.
74. R. Bauernschmitt and R. Ahlrichs, *J. Chem. Phys.*, 1996, **104**, 9047-9052.
75. K. Takatsuka, T. Fueno and K. Yamaguchi, *Theor. Chim. Acta*, 1978, **48**, 175-183.
76. S. Grimme, *Angew. Chem. Int. Ed.*, 2013, **52**, 6306-6312.
77. C. Lee, W. Yang and R. G. Parr, *Phys. Rev. B*, 1988, **37**, 785-789.
78. A. D. Becke, *J. Chem. Phys.*, 1993, **98**, 5648-5652.
79. Y. Zhao, N. E. Schultz and D. G. Truhlar, *J. Chem. Theory Comput.*, 2006, **2**, 364-382.
80. Z. Mou, Y.-H. Tian and M. Kertesz, *Phys. Chem. Chem. Phys.*, 2017, **19**, 24761-24768.
81. M. J. Frisch, G. W. Trucks, H. B. Schlegel, G. E. Scuseria, M. A. Robb, J. R. Cheeseman, G. Scalmani, V. Barone, G. A. Petersson, H. Nakatsuji, X. Li, M. Caricato, A. V. Marenich, J. Bloino, B. G. Janesko, R. Gomperts, B. Mennucci, H. P. Hratchian, J. V. Ortiz, A. F. Izmaylov, J. L. Sonnenberg, Williams, F. Ding, F. Lipparini, F. Egidi, J. Goings, B. Peng, A. Petrone, T. Henderson, D. Ranasinghe, V. G. Zakrzewski, J. Gao, N. Rega, G. Zheng, W. Liang, M. Hada, M. Ehara, K. Toyota, R. Fukuda, J. Hasegawa, M. Ishida, T. Nakajima, Y. Honda, O. Kitao, H. Nakai, T. Vreven, K. Throssell, J. A. Montgomery Jr., J. E. Peralta, F. Ogliaro, M. J. Bearpark, J. J. Heyd, E. N. Brothers, K. N. Kudin, V. N. Staroverov, T. A. Keith, R. Kobayashi, J. Normand, K. Raghavachari, A. P. Rendell, J. C. Burant, S. S. Iyengar, J. Tomasi, M. Cossi, J. M. Millam, M. Klene, C. Adamo, R. Cammi, J. W. Ochterski, R. L. Martin, K. Morokuma, O. Farkas, J. B. Foresman and D. J. Fox, Wallingford, CT, 2016.
82. H. Lischka, T. Müller, P. G. Szalay, I. Shavitt, R. M. Pitzer and R. Shepard, *Wires Comput. Mol. Sci.*, 2011, **1**, 191-199.
83. H. Lischka, R. Shepard, T. Müller, P. G. Szalay, R. M. Pitzer, A. J. A. Aquino, M. M. Araújo do Nascimento, M. Barbatti, L. T. Belcher, J.-P. Blaudeau, I. Borges, Jr., S. R.

Brozell, E. A. Carter, A. Das, G. Gidofalvi, L. González, W. L. Hase, G. Kedziora, M. Kertesz, F. Kossoski, F. B. C. Machado, S. Matsika, S. A. do Monte, D. Nachtigallová, R. Nieman, M. Oppel, C. A. Parish, F. Plasser, R. F. K. Spada, E. A. Stahlberg, E. Ventura, D. R. Yarkony and Z. Zhang, *J. Chem. Phys.*, 2020, **152**.

84. F. Plasser, M. Wormit and A. Dreuw, *J. Chem. Phys.*, 2014, **141**, 024106.
85. F. Plasser, *URL: http://theodore-qc. sourceforge. net*, 2017.
86. F. Plasser and H. Lischka, *J. Chem. Theory Comput.*, 2012, **8**, 2777-2789.
87. S. G. Balasubramani, G. P. Chen, S. Coriani, M. Diedenhofen, M. S. Frank, Y. J. Franzke, F. Furche, R. Grotjahn, M. E. Harding, C. Hättig, A. Hellweg, B. Helmich-Paris, C. Holzer, U. Huniar, M. Kaupp, A. Marefat Khah, S. Karbalaei Khani, T. Müller, F. Mack, B. D. Nguyen, S. M. Parker, E. Perlt, D. Rappoport, K. Reiter, S. Roy, M. Rückert, G. Schmitz, M. Sierka, E. Tapavicza, D. P. Tew, C. van Wüllen, V. K. Voora, F. Weigend, A. Wodyński and J. M. Yu, *J. Chem. Phys.*, 2020, **152**.
88. S. Horn, F. Plasser, T. Müller, F. Libisch, J. Burgdörfer and H. Lischka, *Theor. Chem. Acc.*, 2014, **133**, 1511.